nature immunology

SUPPLEMENTARY INFORMATION

https://doi.org/10.1038/s41590-019-0346-9

In the format provided by the authors and unedited.

Adaptive plasticity of IL-10$^+$ and IL-35$^+$ T_{reg} cells cooperatively promotes tumor T cell exhaustion

Deepali V. Sawant[1,11,14], Hiroshi Yano[1,2,14], Maria Chikina[3], Qianxia Zhang[1,12], Mengting Liao[1,13], Chang Liu[1], Derrick J. Callahan[1,2], Zhe Sun[4], Tao Sun[4], Tracy Tabib[5], Arjun Pennathur[6], David B. Corry[7], James D. Luketich[6], Robert Lafyatis[5], Wei Chen[4], Amanda C. Poholek[1,8], Tullia C. Bruno[1,9,10], Creg J. Workman[1] and Dario A. A. Vignali[1,9,10]*

[1]Department of Immunology, University of Pittsburgh School of Medicine, Pittsburgh, PA, USA. [2]Program in Microbiology and Immunology, University of Pittsburgh School of Medicine, Pittsburgh, PA, USA. [3]Department of Computational and Systems Biology, University of Pittsburgh School of Medicine, Pittsburgh, PA, USA. [4]Department of Biostatistics, University of Pittsburgh School of Public Health, Pittsburgh, PA, USA. [5]Division of Rheumatology and Clinical Immunology, Department of Medicine, University of Pittsburgh School of Medicine, Pittsburgh, PA, USA. [6]Department of Cardiothoracic Surgery, University of Pittsburgh School of Medicine and University of Pittsburgh Medical Center, Pittsburgh, PA, USA. [7]Department of Medicine, Baylor College of Medicine, Houston, TX, USA. [8]Department of Pediatrics, University of Pittsburgh School of Medicine, Pittsburgh, PA, USA. [9]Tumor Microenvironment Center, UPMC Hillman Cancer Center, Pittsburgh, PA, USA. [10]Cancer Immunology & Immunotherapy Program, UPMC Hillman Cancer Center, Pittsburgh, PA, USA. [11]Present address: Department of Inflammation and Oncology, Discovery Research, Amgen, South San Francisco, CA, USA. [12]Present address: Evergrande Center for Immunologic Diseases and Ann Romney Center for Neurologic Diseases, Harvard Medical School and Brigham and Women's Hospital, Boston, MA, USA. [13]Present address: The Third Xiangya Hospital, Central South University, Changsha, Hunan, China. [14]These authors contributed equally: Deepali V. Sawant, Hiroshi Yano. *e-mail: dvignali@pitt.edu

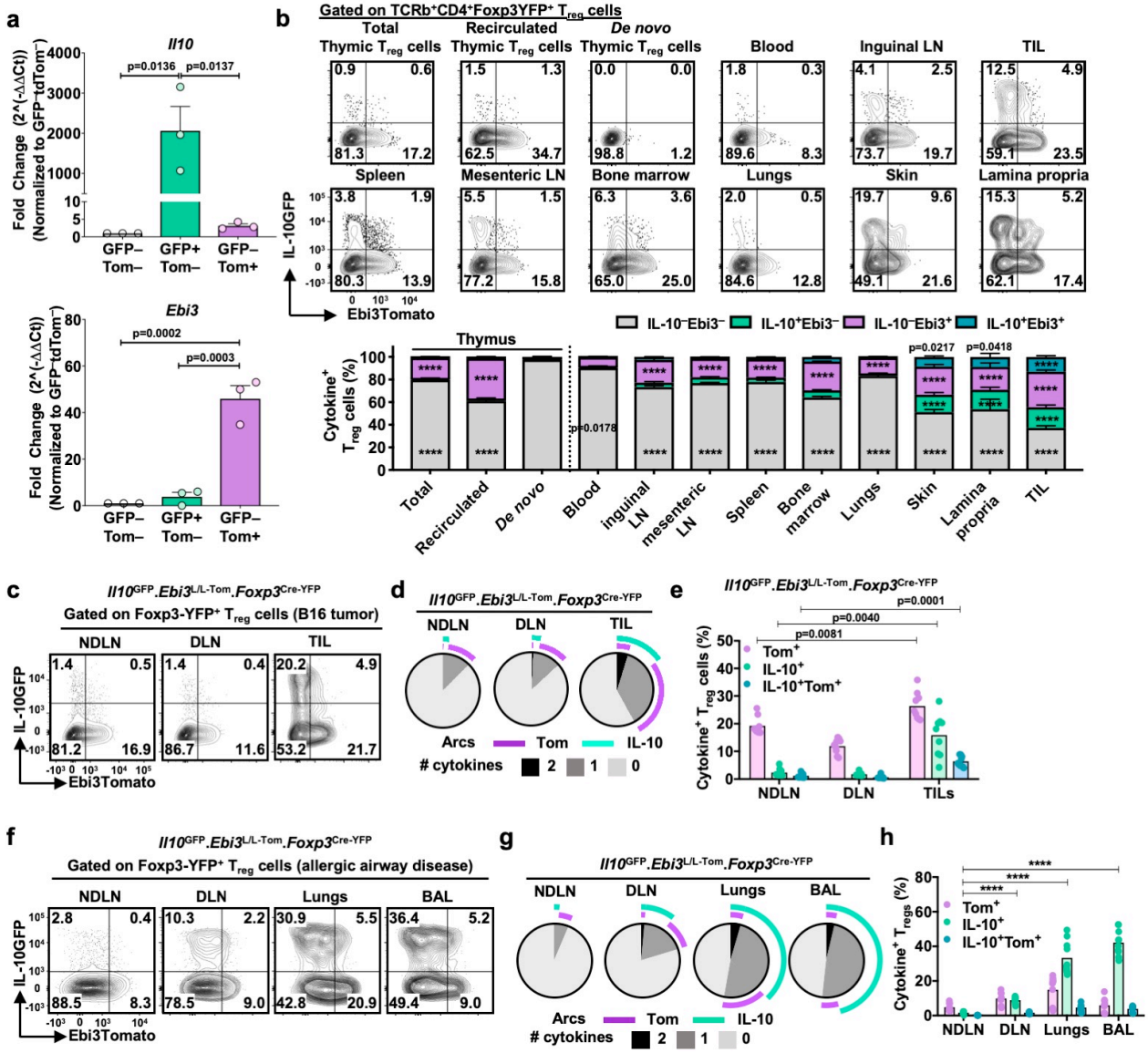
a
Il10
p=0.0136
p=0.0137
Fold Change (2^(-ΔΔCt)) (Normalized to GFP⁻tdTom⁻)
GFP– Tom–
GFP+ Tom–
GFP– Tom+
Ebi3
p=0.0002
p=0.0003
b
Gated on TCRb⁺CD4⁺Foxp3YFP⁺ Treg cells
Total Thymic Treg cells
Recirculated Thymic Treg cells
De novo Thymic Treg cells
Blood
Inguinal LN
TIL
Spleen
Mesenteric LN
Bone marrow
Lungs
Skin
Lamina propria
IL-10GFP
Ebi3Tomato
IL-10⁻Ebi3⁻
IL-10⁺Ebi3⁻
IL-10⁻Ebi3⁺
IL-10⁺Ebi3⁺
Thymus
Cytokine⁺ Treg cells (%)
p=0.0178
p=0.0217
p=0.0418
Total
Recirculated
De novo
Blood
inguinal LN
mesenteric LN
Spleen
Bone marrow
Lungs
Skin
Lamina propria
TIL
c
Il10GFP.Ebi3L/L-Tom.Foxp3Cre-YFP
Gated on Foxp3-YFP⁺ Treg cells (B16 tumor)
NDLN
DLN
TIL
d
NDLN
DLN
TIL
Arcs
Tom
IL-10
cytokines
2
1
0
e
p=0.0001
p=0.0040
p=0.0081
Tom⁺
IL-10⁺
IL-10⁺Tom⁺
Cytokine⁺ Treg cells (%)
NDLN
DLN
TILs
f
Gated on Foxp3-YFP⁺ Treg cells (allergic airway disease)
NDLN
DLN
Lungs
BAL
g
NDLN
DLN
Lungs
BAL
Arcs
Tom
IL-10
cytokines
h
Tom⁺
IL-10⁺
IL-10⁺Tom⁺
Cytokine⁺ Tregs (%)
NDLN
DLN
Lungs
BAL

8976Supplementary Figure 1

Distribution and characterization of IL-10- and IL-35-expressing T_{reg} cells in inflammatory environments

a, Validation of fluorescent reporters by real-time RT-PCR. Splenic T_{reg} cell subpopulations were sorted from *Il10*^{GFP}.*Ebi3*^{Tom}.*Foxp3*$^{Cre\text{-}YFP}$ mice, and *Il10* and *Ebi3* transcripts were analyzed. Relative fold change expression was determined by normalizing to GFP^{-}Tom^{-} double-negative T_{reg} cells. Data averaged from 3 independent experiments. Statistical significance was determined by One-way ANOVA with Holm-Sidak multiple comparisons (*P* values as indicated).

b, Representative flow plots depicting the expression of IL-10 and Ebi3 in T_{reg} cells isolated from the indicated tissues of 8wks old naive *Il10*^{GFP}.*Ebi3*^{Tom}.*Foxp3*$^{Cre\text{-}YFP}$ mice (*top*). Stacked-bar graph depicting the percent distribution of subpopulations (*bottom*). Recirculating (CD62L$^{+/-}$Nrp1^{+}) and *de novo* (CD62L^{+}Nrp1^{-}) T_{reg} cells for Thymus. Data were averaged from 2 independent experiments with *n*=5 mice per tissue, except for thymus, blood, and lamina propria (n=3). Error bars represent s.e.m. Statistical significance was determined by comparing tissues to *de novo* Thymus with Two-way ANOVA with Holm-Sidak multiple comparisons (****p<0.0001 and other *P* values as indicated).

c, Representative flow plots depicting expression of IL-10^{+} and Tom^{+} cells within Foxp3-YFP^{+} T_{reg} cells isolated from day 14 B16 tumor-bearing *Il10*^{GFP}.*Ebi3*$^{L/L\text{-}Tom}$.*Foxp3*$^{Cre\text{-}YFP}$ mice. CD4^{+}YFP^{+} T_{reg} cells were assessed for the expression of IL-10 and Tom in NDLN, DLN and TIL.

d, SPICE plots depicting co-expression pattern of IL-10 and Tom on TIL T_{reg} cells from B16 tumor-bearing *Il10*^{GFP}.*Ebi3*$^{\mathbf{L/L\text{-}Tom}}$.*Foxp3*$^{Cre\text{-}YFP}$ mice as in (***c***). Data averaged from 3 independent experiments with n=9 mice total.

e, Scatter-bar plot depicting percent distribution of T_{reg} cell subpopulations as in (***c***). Bars represent mean values.

f, Representative flow plots depicting the distribution of IL-10^{+} and Tom^{+} cells within Foxp3-YFP^{+} T_{reg} cells isolated from d14 allergic inflammation induced *Il10*^{GFP}.*Ebi3*$^{L/L\text{-}Tom}$.*Foxp3*$^{Cre\text{-}YFP}$ mice.

g, SPICE plots depicting co-expression pattern of IL-10 and Tom on T_{reg} cells as described in (***f***). Data averaged from 3 independent experiments with n=10 mice total.

h, Scatter-bar plot depicting percent distribution of T_{reg} cell subpopulations as in (***f***). Bars represent mean values.

(**e** and **h**) Statistical significance was determined by Two-way ANOVA with Holm-Sidak multiple comparisons (****p<0.0001 and other *P* values as indicated).

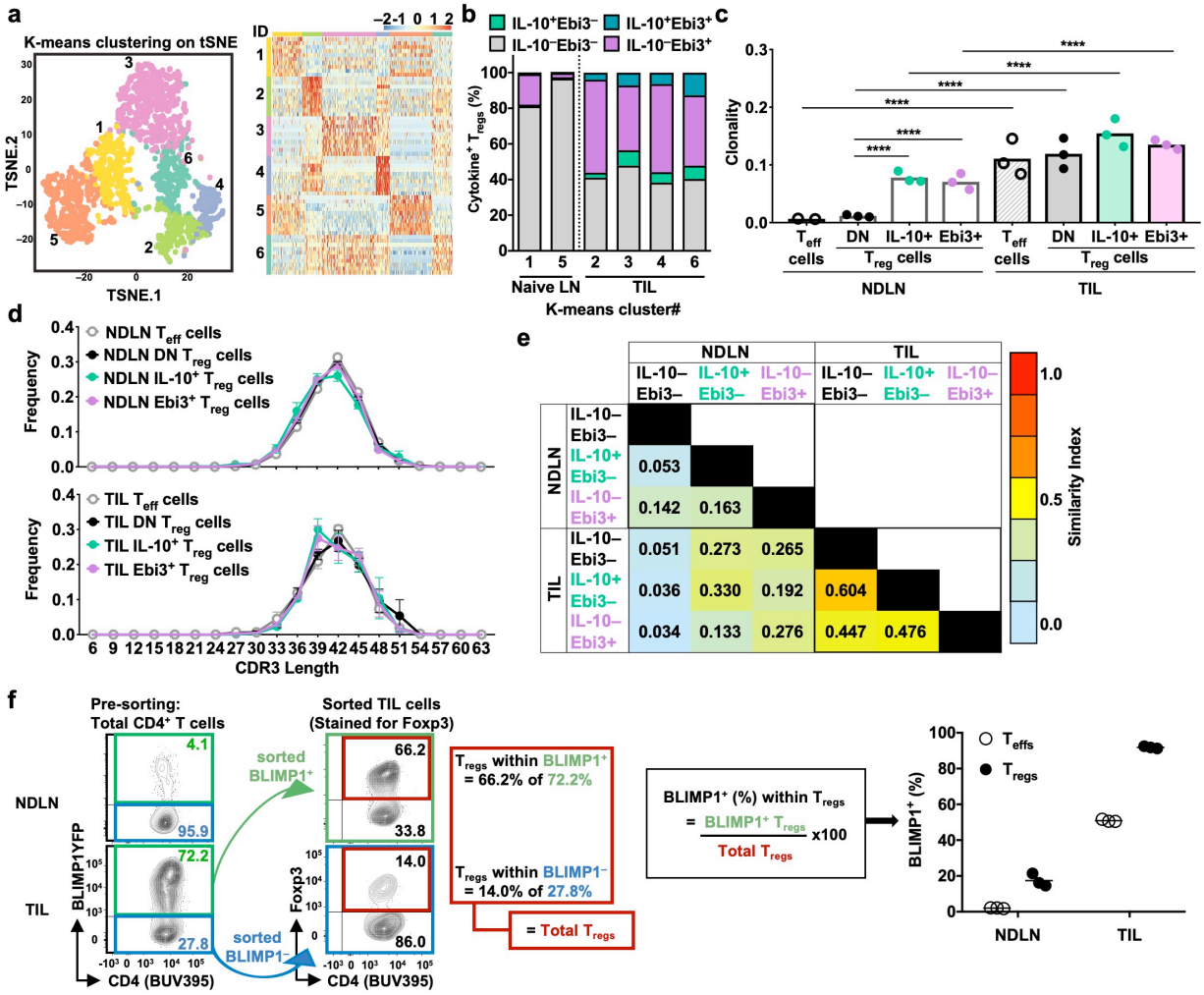

Supplementary Figure 2

Substantial TCR clonal overlap among intratumoral T_{reg} cell subpopulations, consistent with lack of distinct transcriptomic signatures

a, scRNAseq tSNE plots of bulk T_{reg} cells from naive LNs and day 14 B16 Tumors (TIL T_{reg} cells) from *Foxp3*$^{Cre\text{-}YFP}$ mice, with unsupervised K-means clustering (*left*) and a heat map depicting the top 10 differentially expressed genes for each of the 6 clusters identified (*right*).

b, Stacked-bar graph depicting the percent distribution of T_{reg} cell subpopulations within each cluster identified as in (***a***).

c, Clonality was determined by examining the degree of TCR diversity within each population by TCRseq. Productive CDR3 sequences were used to define the TCR diversity. The indicated Teff control and T_{reg} cell subpopulations were FACS sorted from day 14 B16 tumor-bearing *Il10*^{GFP}.*Ebi3*^{Tom}.*Foxp3*$^{Cre\text{-}YFP}$ mice for genomic DNA purification. Bars represent mean values. Statistical significance was determined by One-way ANOVA with with Holm-Sidak multiple comparisons (****p<0.0001).

d, Line graphs representing the mean length of productive CDR3 locus sequence comparing the T_{reg} cells subpopulations and effector T cells. Error bars represent s.e.m.

e, TCR clonal similarity was determined by Morisita-Horn similarity index cross-examining the productive CDR3 sequences of Teff control and T_{reg} cell subpopulations. Representative of three independent mouse samples is shown.

(**c-e**) Data combined from TCR-sequencing data from three separate, individual *Il10*^{GFP}.*Ebi3*^{Tom}.*Foxp3*$^{Cre\text{-}YFP}$ mice. Error bars represent s.e.m.

f, Representative flow plots depicting the BLIMP1YFP expression level plotted against CD4. (*left*): BLIMP1YFP^{-} and BLIMP1YFP^{+} fractions of CD4^{+} TILs were purified by FACS sorting from d14 B16 tumor-bearing Prdm1^{YFP} transgenic mice, followed by intracellular Foxp3 staining of the sorted cells. Data averaged from three sets of tumors with three tumors per set pooled for sorting. (*right*): Scatter plot depicting the percent distribution of BLIMP1YFP^{+} T_{effs} and T_{reg} cells.

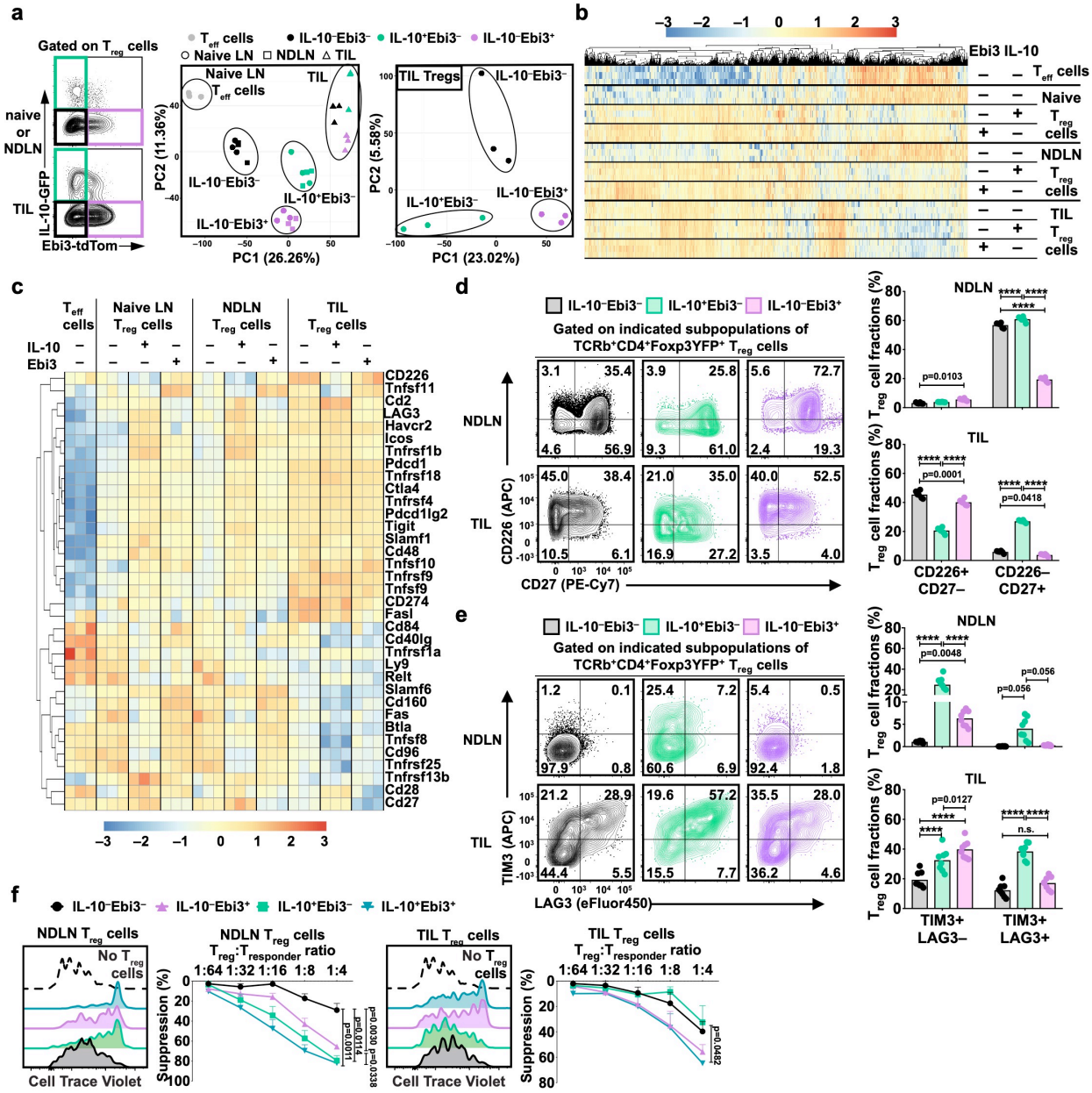

Supplementary Figure 3

Global transcriptomic analysis of intratumoral T_{reg} cell subpopulations

a, (*left*) Representative gating strategy for T_{reg} cell subpopulation sorting for RNAseq. Each population was double-sorted. (*right*) PCA plot demonstrating the segregation of naive LN, NDLN, and B16 tumor derived TIL T_{reg} cell subpopulations isolated from B16 tumor-bearing *Il10*^{GFP}.*Ebi3*^{Tom}.*Foxp3*$^{Cre\text{-}YFP}$ mice defined by their IL-10 and IL-35 expression pattern (IL-10^{-}Ebi3^{-}, IL-10^{+}Ebi3^{-}, and IL-10^{-}Ebi3^{+}) as well as naive LN effector T cell control (*left PCA*). A separate PCA plot was generated depicting only TIL T_{reg} cell populations (*right PCA*). Data generated from three independent sequencing runs. Samples pooled from 4 mice per experiment to sort T_{reg} cell subpopulations. Each dot in PCA plots represent individual sequencing run. For statistical analysis q-value FDR of 0.05 was used to

determine the confidence of adjusted *P* values.

b, Heat map of top 5,000 differentially expressed genes representing cross-examination of Treg cell subpopulations as in (***a***).

c, Heat map of differentially expressed co-signaling molecules contrasting naive LN T_{eff} cells and T_{reg} cell subpopulations. Only genes that showed significant overall changes are listed.

d, Representative flow plots depicting the expression of CD226 and CD27. Scatter-bar graphs demonstrating T_{reg} cells differentially distributed based on the reciprocal expression of CD226 and CD27.

e, Representative flow plots depicting the expression of TIM3 and LAG3. Scatter-bar graphs demonstrating T_{reg} cells differentially distributed between TIM3 single positive and $TIM3^{+}LAG3^{+}$ expression pattern.

(**d-e**) Data averaged from 2 independent experiments with n=7 mice. Statistical significance was determined by Two-way ANOVA with Holm-Sidak multiple comparisons (****p<0.0001 and other *P* values indicated).

f, Microsuppression assay comparing the suppressive function of T_{reg} cell subpopulations (*top*: NDLN Treg cells, *bottom*: TIL T_{reg} cells). Representative half-offset histograms show the proliferation of $CD4^{+}Foxp3^{-}$ Teff responder ($T_{responder}$) cells assessed by the decay of Cell Trace Violet proliferation dye at 1:4 T_{reg}:$T_{responder}$ ratio. Line graphs depicting the summary of 3 independent experiments. Two-way ANOVA with Holm-Sidak multiple comparisons (*P* values indicated in the graphs).

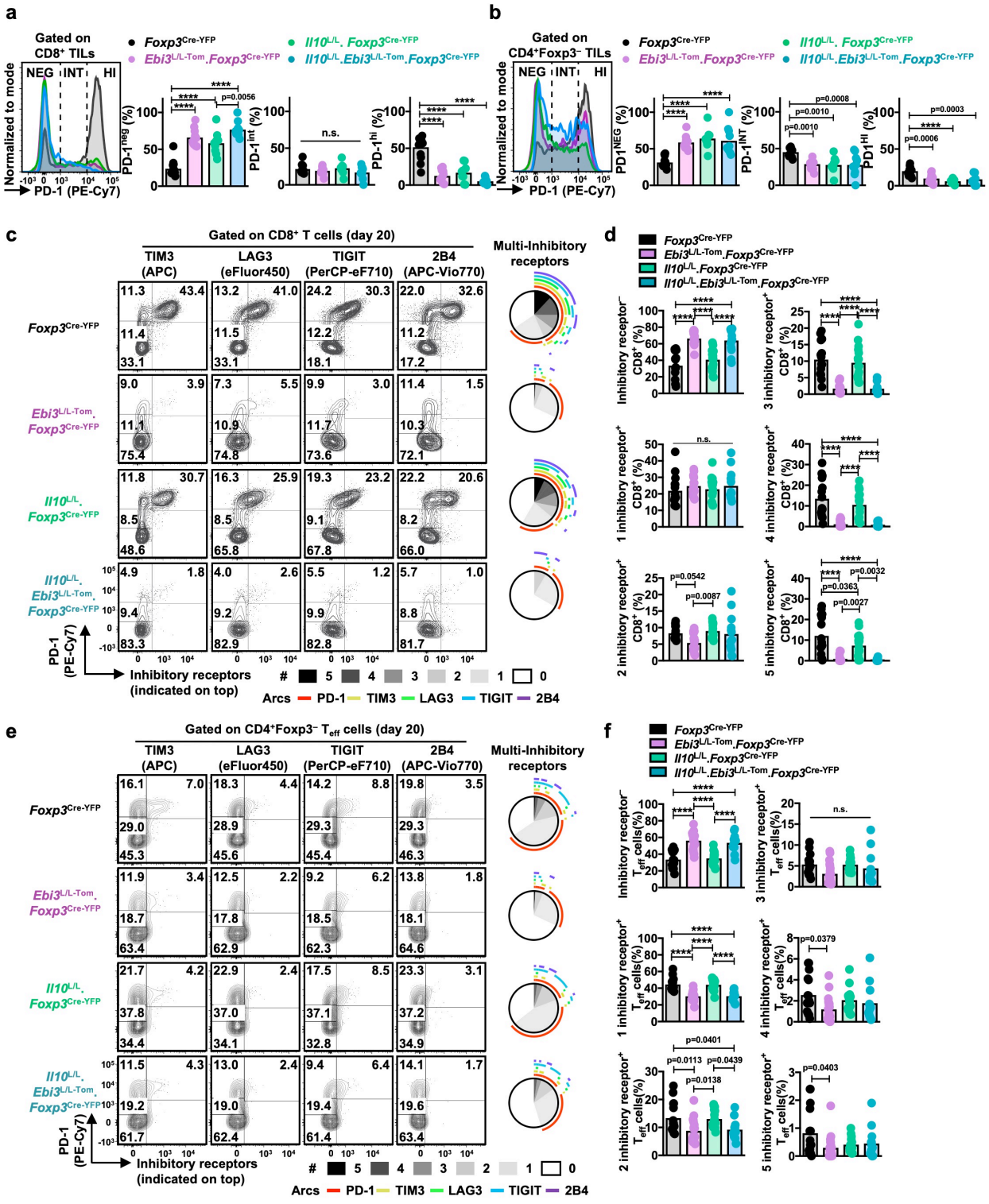

Supplementary Figure 4

Modulation of inhibitory receptor expression in CD4$^+$ and CD8$^+$ TILs by T_{reg} cell-derived IL-10 and IL-35

a, Representative histograms depicting PD-1 expression on B16 tumor-infiltrating CD8$^+$ TILs from *Foxp3*$^{Cre\text{-}YFP}$ (n=13), *Il10*$^{L/L}$.*Foxp3*$^{Cre\text{-}}$

^{YFP} (n=9), *Ebi3*$^{L/L\text{-}Tom}$.*Foxp3*$^{Cre\text{-}YFP}$ (n=11), and *Il10*$^{L/L}$.*Ebi3*$^{L/L\text{-}Tom}$.*Foxp3*$^{Cre\text{-}YFP}$ (n=10) mice at day 14 post tumor inoculation. Scatter-bar graphs depicting percent distribution of PD-1^{neg}, PD-1^{int}, and PD-1^{hi} CD8^{+} TILs.

b, Representative histograms depicting the PD-1 expression on CD4^{+}Foxp3^{-} T cells isolated from B16 tumor-bearing mice as in (***a***). Scatter-bar graphs depicting percent distribution of PD-1^{neg}, PD-1^{int}, and PD-1^{hi} CD4^{+}Foxp3^{-} T_{eff} cells.

(**a-b**) Data averaged from 3 independent experiments. Statistical significance was determined by One-way ANOVA with Holm-Sidak multiple comparison (****p<0.0001 and other *P* values as indicated).

c, Representative flow plots depicting the expression of inhibitory receptors (PD-1, TIM3, LAG3, TIGIT, and 2B4) on CD8^{+} T cells from day 20 B16 tumor-bearing *Foxp3*$^{Cre\text{-}YFP}$ (n=15), *Il10*$^{L/L}$.*Foxp3*$^{Cre\text{-}YFP}$ (n=20), *Ebi3*$^{L/L\text{-}Tom}$.*Foxp3*$^{Cre\text{-}YFP\ YFP}$ (n=17), and *Il10*$^{L/L}$.*Ebi3*$^{L/L\text{-}Tom}$.*Foxp3*$^{Cre\text{-}YFP\ YFP}$ (n=13) mice. SPICE plots depicting co-expression pattern of multiple inhibitory receptors.

d, Scatter-bar graphs representing the percent distribution of inhibitory receptor-negative (0 & 1 inhibitory receptor-expressing effector-like) and multi-inhibitory receptor^{+} (3-5 inhibitory receptor-expressing exhausted) CD8^{+} T cells as in (***c***).

e, Representative flow plots depicting expression of inhibitory receptors (PD-1, TIM3, LAG3, TIGIT, and 2B4) on CD4^{+}Foxp3^{-} T_{eff} cells from day 20 B16 tumor-bearing mice as in (***c***). SPICE plots depicting co-expression pattern of multiple inhibitory receptors.

f, Scatter-bar graphs representing the percent distribution of inhibitory receptor-negative (0 & 1 inhibitory receptor-expressing effector-like) and multi-inhibitory receptor^{+} (3—5 inhibitory receptor-expressing exhausted) CD4^{+}Foxp3^{-} TILs as in (***e***). Statistical significance was determined by One-way ANOVA with Holm-Sidak multiple comparison (****p<0.0001 and other *P* values as indicated).

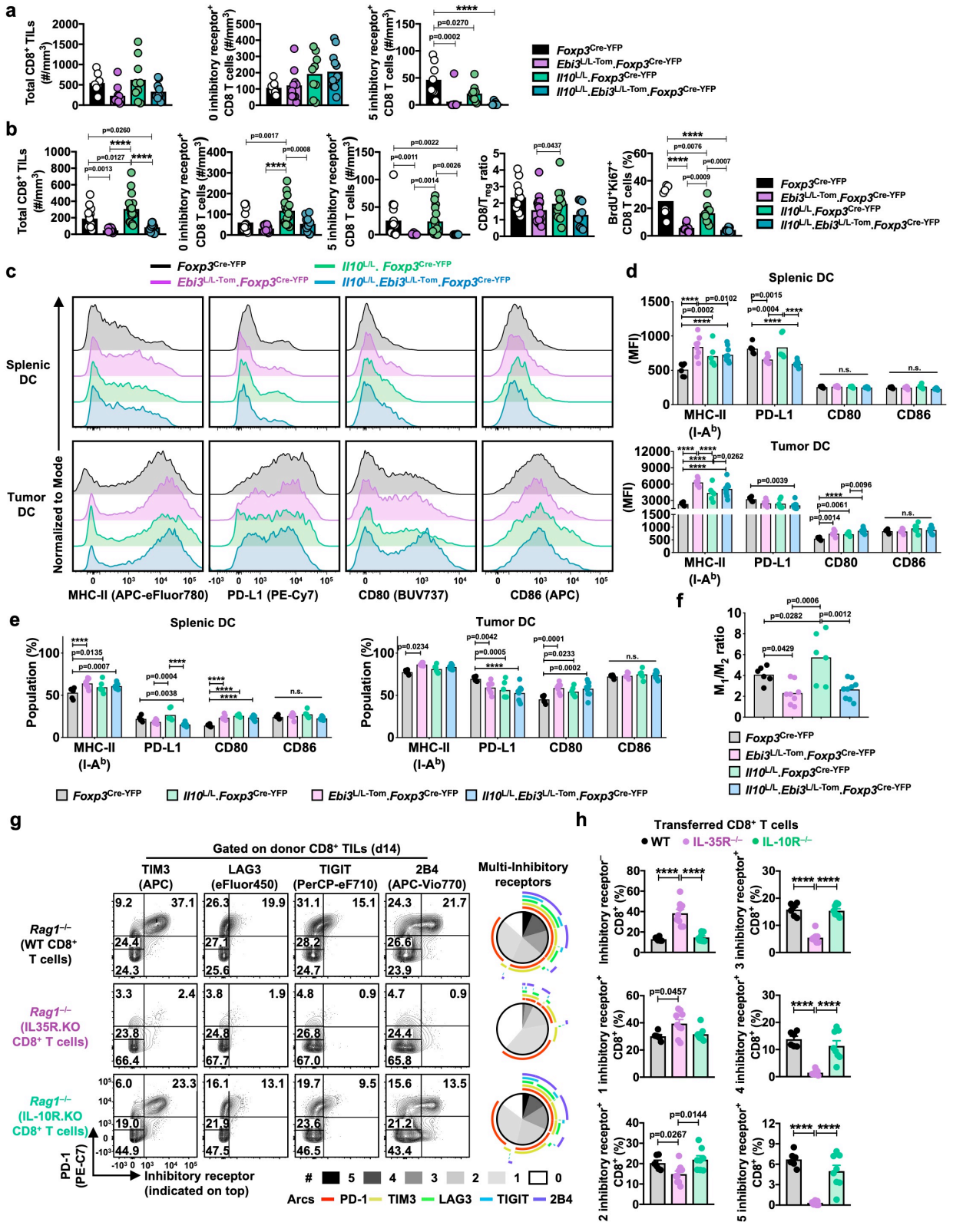

Supplementary Figure 5

Differential regulation of the tumor microenvironment by T_{reg} cell-derived IL-10 and IL-35

a, Scatter-bar graphs depicting the absolute number of $CD8^+$ TILs normalized to tumor volumes (either total, 0inhibitory $receptor^+$, or 5inhibitory $receptors^+$) isolated from day 14 B16 tumor-bearing *Foxp3*$^{Cre\text{-}YFP}$ (n=8), *Il10*$^{L/L}$.*Foxp3*$^{Cre\text{-}YFP}$ (n=9), *Ebi3*$^{L/L\text{-}Tom}$.*Foxp3*$^{Cre\text{-}YFP}$, (n=10) and *Il10*$^{L/L}$.*Ebi3*$^{L/L\text{-}Tom}$.*Foxp3*$^{Cre\text{-}YFP}$ (n=12) mice.

b, Scatter-bar graphs depicting absolute number of $CD8^+$ TILs (either total $CD8^+$ TILs, 0inhibitory $receptor^+$, or 5inhibitory $receptors^+$) normalized to tumor volume, $CD8/T_{reg}$ cell ratio, and $Brdu^+Ki67^+$ proliferating $CD8^+$ TILs from day 20 B16 tumor-bearing *Foxp3*$^{Cre\text{-}YFP}$ (n=15), *Il10*$^{L/L}$.*Foxp3*$^{Cre\text{-}YFP}$ (n=20), *Ebi3*$^{L/L\text{-}Tom}$.*Foxp3*$^{Cre\text{-}YFP}$ (n=17), and *Il10*$^{L/L}$.*Ebi3*$^{L/L\text{-}Tom}$.*Foxp3*$^{Cre\text{-}YFP}$ (n=13) mice.

(**a-b**) Data averaged from 3 independent experiments. Bars represent mean values. Statistical significance was determined by One-way ANOVA with Holm-Sidak multiple comparisons (****p<0.0001 and other *P* values as indicated).

c, Representative histograms depicting expression of indicated markers on splenic and tumor-infiltrating DCs from B16 tumor-bearing *Foxp3*$^{Cre\text{-}YFP}$ (n=6), *Il10*$^{L/L}$.*Foxp3*$^{Cre\text{-}YFP}$ (n=8), *Ebi3*$^{L/L\text{-}Tom}$.*Foxp3*$^{Cre\text{-}YFP}$ (n=6), and *Il10*$^{L/L}$.*Ebi3*$^{L/L\text{-}Tom}$.*Foxp3*$^{Cre\text{-}YFP}$ (n=9) mice.

d, Scatter-bar graphs depicting the Mean Fluorescent Intensity (MFI) of the markers examined as in (**c**).

e, Scatter-bar graphs depicting the percent distribution of indicated markers on splenic and tumor-infiltrating DCs examined as in (**c**).

f, Scatter-bar graphs demonstrating the M_1 vs M_2 subpopulation ratio within the tumor associated macrophage (TAM) population. Statistical significance was determined by One-way ANOVA with Holm-Sidak multiple comparisons (*P* values as indicated).

(**c-f**) Data averaged from 2 independent experiments. Bars represent mean values.

(**c-e**) Statistical significance was determined by Two-way ANOVA with Holm-Sidak multiple comparisons (****p<0.0001 and other p-values as indicated).

g, Representative flow plots depicting the expression of inhibitory receptors and SPICE plots showing the multi-inhibitory receptor co-expression pattern on the donor $CD8^+$ T cells infiltrating B16 tumor-bearing reconstituted *Rag1*$^{-/-}$ mice 14 days post-tumor inoculation as described in **Fig. 5a**.

h, Scatter-bar graphs representing the percent distribution of donor $CD8^+$ TILs based on the number of inhibitory receptors expressed. (WT: n=10, IL-$10R^{-/-}$: n=6, IL-$35R^{-/-}$: n=7). Bars represent mean values. Statistical significance was determined by One-way ANOVA with Holm-Sidak multiple comparisons (****p<0.0001 and other *P* values indicated).

(**g-h**) Data averaged from 2 independent experiments.

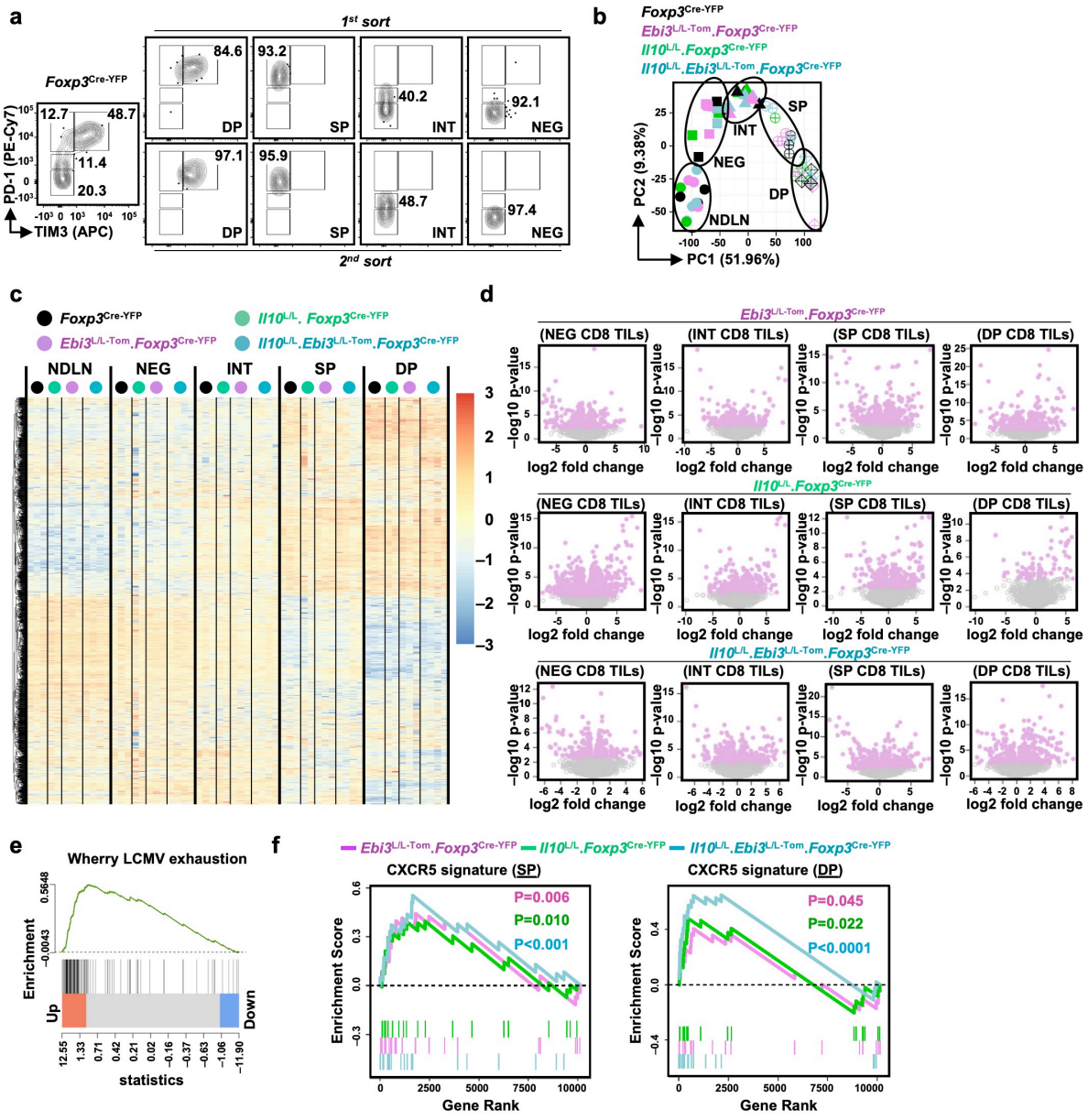

Supplementary Figure 6

Transcriptional analysis of CD8$^+$ TIL subsets from IL-10/IL-35 T$_{reg}$ cell-deficient tumor microenvironments

a, Double-sorting scheme used to fractionate the CD8$^+$ TIL subsets from the control *Foxp3*$^{Cre-YFP}$ and T$_{reg}$ cell-cytokine deficient environments into the NEG, INT, SP and DP fractions. Total CD8$^+$ T cells were sorted from the NDLN for each of the 4 genotypes. Data represent at least 5 independent RNAseq experiments.

b, PCA depicting the NDLN and CD8$^+$ TILs subsets (NEG, INT, SP and DP) isolated from day 14 B16 tumor-bearing *Foxp3*$^{Cre-YFP}$ (n=3), *Il10*$^{L/L}$.*Foxp3*$^{Cre-YFP}$ (n=2), *Ebi3*$^{L/L-Tom}$.*Foxp3*$^{Cre-YFP}$ (n=3), and *Il10* $^{L/L}$.*Ebi3*$^{L/L-Tom}$.*Foxp3*$^{Cre-YFP}$ (n=4) mice. Each of symbol represent an independent RNAseq run replicate.

c, Heat map of top 5,000 differentially expressed genes representing $CD8^+$ TILs from NDLN and NEG, INT, SP, and DP subsets. Genes were considered differentially expressed if their q-value FDR was below 0.05.

d, Volcano plots contrasting $CD8^+$ TIL subpopulations (NEG = PD-1^{neg}, INT = PD-1^{int}, SP = PD-$1^{hi}TIM3^-$, DP = PD-$1^{hi}TIM3^+$) isolated from *Il10*$^{L/L}$.*Foxp3*$^{Cre\text{-}YFP}$, *Ebi3*$^{L/L\text{-}Tom}$.*Foxp3*$^{Cre\text{-}YFP}$, and *Il10*$^{L/L}$.*Ebi3*$^{L/L\text{-}Tom}$.*Foxp3*$^{Cre\text{-}YFP}$ mice against the corresponding populations from *Foxp3*$^{Cre\text{-}YFP}$ control mice. Colored dots represent genes with q-value false discovery rate of <0.05.

e, GSEA plot depicting the comparison of the exhaustion program in chronic LCMV infection versus the tumor exhaustion signature (derived by PD-1^{hi} to PD-1^{neg} $CD8^+$ T cell comparison), with *P* values as indicated.

f, GSEA plot depicting the gene signature of PD-1 checkpoint blockade responsive $TCF1^+CXCR5^+$ $CD8^+$ T cell subset in SP $CD8^+$ TILs (*left*) and DP $CD8^+$ TILs (*right*) from cytokine deficient-T_{reg} cell environments (*Il10*$^{L/L}$.*Foxp3*$^{Cre\text{-}YFP}$, *Ebi3*$^{L/L\text{-}Tom}$.*Foxp3*$^{Cre\text{-}YFP}$, and *Il10*$^{L/L}$.*Ebi3*$^{L/L\text{-}Tom}$.*Foxp3*$^{Cre\text{-}YFP}$); *P* values as indicated.

(**e-f**) Statistical significance was determined by the rankSumTestWithCorrelation test implemented in the limma package with correction for loss in degrees of freedom due to correlation among genes. All *P* values are two sided. No correction for multiple hypothesis was performed.

(**a-f**) Data are averaged from at least 5 independent RNASeq experiments with genotype-specific $CD8^+$ T cell replicates as indicated - *Foxp3*$^{Cre\text{-}YFP}$ (n=3), *Il10*$^{L/L}$.*Foxp3*$^{Cre\text{-}YFP}$ (n=2), *Ebi3*$^{L/L\text{-}Tom}$.*Foxp3*$^{Cre\text{-}YFP}$ (n=3), and *Il10* $^{L/L}$.*Ebi3*$^{L/L\text{-}Tom}$.*Foxp3*$^{Cre\text{-}YFP}$ CD8s (n=4).

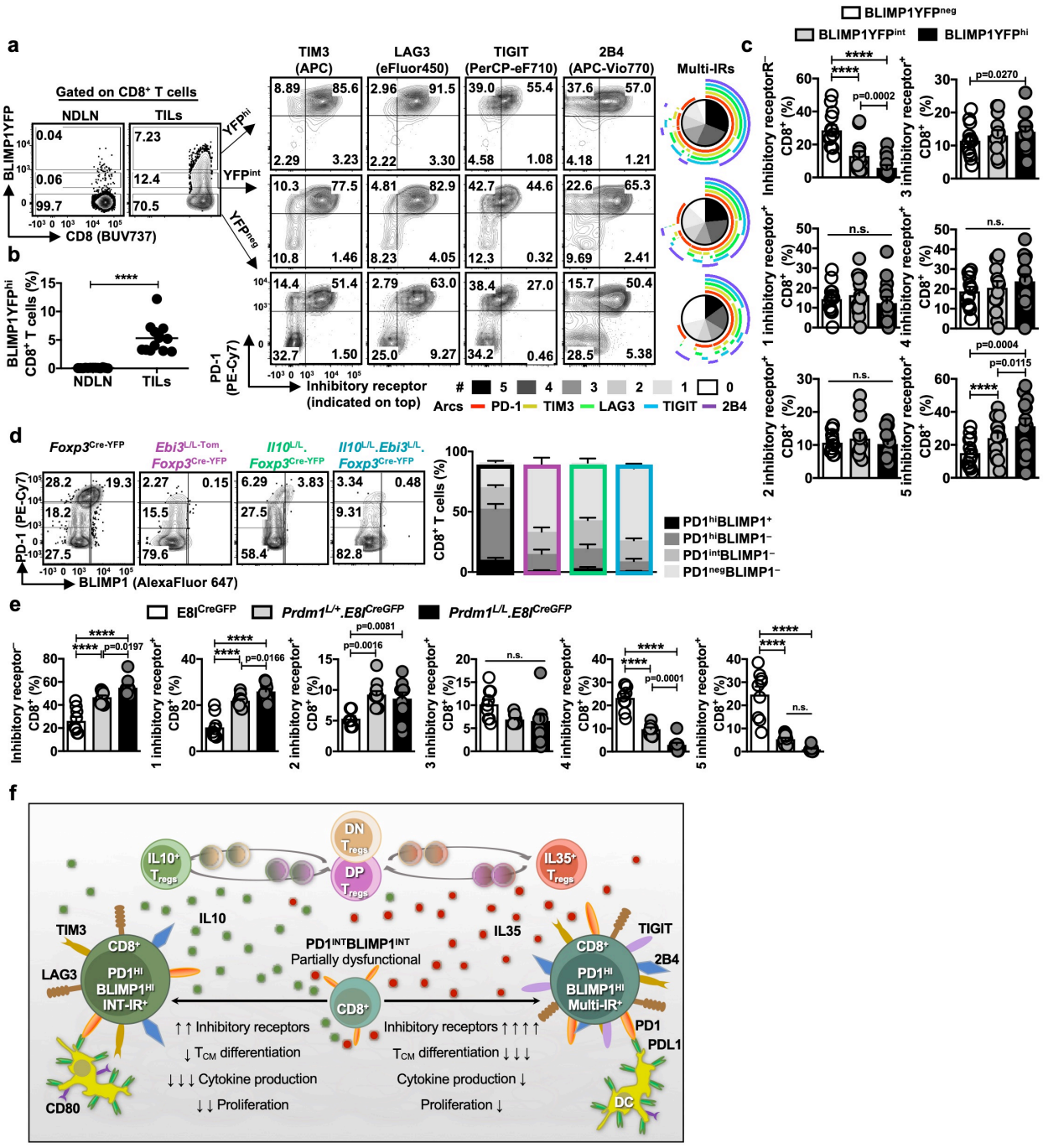

Supplementary Figure 7

IL-10^{+} and IL-35^{+} T$_{reg}$ cells drive BLIMP1 induction on TILs *in vivo*

a, Representative flow plots depicting the expression of BLIMP1YFP expression levels in NDLN and TIL CD8^{+} T cells from B16 tumor-bearing Prdm1^{YFP} transgenic reporter mice (n=13). CD8^{+} TILs representative flow and SPICE plots demonstrating the expression of inhibitory receptors on the BLIMP1YFP^{hi}, YFP^{int} and YFP^{neg} CD8^{+} T cell fractions.

b, Scatter plots showing the percent distribution of YFP^{hi} subpopulation among CD8^{+} T cells as in **(a)**. Statistical significance was

determined by paired two-tailed Student's t-test (****p<0.0001).

c, Scatter-bar graphs depicting the percent distribution of $CD8^+$ TILs based on the number of inhibitory receptors expressed as in **(a)**. Bars represent mean values. Statistical significance was determined by One-way ANOVA with Holm-Sidak multiple comparison (****p<0.0001 and other *P* values as indicated).

(**a-c**) Data averaged from 3 independent experiments, with n=13 mice/group.

d, Representative flow plots depicting the protein level expression pattern of PD-1 and BLIMP1 on $CD8^+$ T cells from B16 tumor-bearing *Foxp3*$^{Cre\text{-}YFP}$ (n=14), *Il10*$^{L/L}$.*Foxp3*$^{Cre\text{-}YFP}$ (n=11), *Ebi3*$^{L/L\text{-}Tom}$.*Foxp3*$^{Cre\text{-}YFP}$ (n=12), and *Il10*$^{L/L}$.*Ebi3*$^{L/L\text{-}Tom}$.*Foxp3*$^{Cre\text{-}YFP}$ (n=14) mice, with stacked bar graph depicting percent distribution of PD-1^{hi}, PD-1^{int}, and PD-1^{neg} $CD8^+$ T cells co-expressing PD-1 and BLIMP1. Data averaged from 3 independent experiments.

e, Scatter-bar graphs representing the percent distribution of $CD8^+$ T cells expressing 0-5 inhibitory receptors from B16 tumor-bearing E8I$^{Cre\text{-}GFP}$ (n=9), *Prdm1*$^{L/+}$.E8I$^{Cre\text{-}GFP}$ (n=12), and *Prdm1*$^{L/L}$.E8I$^{Cre\text{-}GFP}$ (n=10) mice as in **Fig. 7d**. Data averaged from 3 independent experiments. Bars represent mean values. Statistical significance was determined by One-way ANOVA with Holm-Sidak multiple comparison (****p<0.0001 and other *P* values as indicated).

g, Graphical summary of the regulatory functions of T_{reg}-derived IL-10 and IL35 depicted by their common and non-redundant effects on TILs. T_{reg}-derived IL35 predominantly regulated IR-expression and T_{CM} differentiation while T_{reg}-derived IL-10 played a greater role in limiting cytokine production and proliferation of $CD8^+$ TILs.